Available online at www.sciencedirect.com
SCIENCE DIRECT
Catalysis Today 105 (2005) 484–491
CATALYSIS TODAY
www.elsevier.com/locate/cattod

Characteristics of drying and active component distribution in alumina monoliths using ^{1}H-NMR imaging

Z.R. Ismagilov [a,*], S.A. Yashnik [a], A.A. Matveev [b], I.V. Koptyug [b], J.A. Moulijn [c]

[a] *Boreskov Institute of Catalysis, 630090 Novosibirsk, Russian Federation, Russia*
[b] *International Tomography Center, Novosibirsk, Russia*
[c] *Delft University of Technology, Delft, The Netherlands*

Abstract

The distribution of water in the impregnated monolithic substrates was visualized by ^{1}H-NMR imaging. The two-dimensional water content maps along the axial and radial directions have been collected for different monoliths at variation of the drying conditions. Using the blow-through air for drying of the substrate with coated external walls and with free access of air to external walls leads to the parabolic profile of water concentration along the axial direction of the sample. Drying of the monoliths with open external walls proceeds more uniformly in the radial and axial directions of the substrate. Characteristics of drying of alumina monoliths, calcined at 600, 900 and 1200 °C having differences in the pore structure and pore distribution, are studied.

During drying of the impregnated washcoated monolith the certain part of the introduced active component precursor (H_2PtCl_6 or H_2PdCl_4) is transported from the substrate macropores to the mesoporous washcoated layer which leads to enrichment of the washcoat of the final catalyst by active component. The non-destructive character of ^{1}H-NMR microimaging demonstrated its capability to visualize the water content maps in monoliths in the presence of Pt and Pd.

Keywords: ^{1}H-NMR imaging; Honeycomb monolith; Incipient wetness impregnation; Drying; Active component distribution

1. Introduction

The active component distribution in the impregnated honeycomb monolithic catalysts is usually formed at the drying stage. This is caused by redistribution of the impregnating solution containing the active component precursor in the pore space of the support during drying, which depends both on the properties of the impregnating solution and on the pore structure of the support. It is worth to note that we used this model keeping in mind that it applies only for ''loosely'' bound active component precursors.

There are two main groups of ceramic and oxide monolithic substrates [1,2]. The first group includes monoliths with well developed specific surface area (more than 70–100 m^2/g) and pore structure: for example, substrates on the basis of γ-Al_2O_3 [1,2], which are traditionally used for the synthesis of catalysts by the incipient wetness impregnation [1–3]. The second group consists of substrates with a surface area less than 10–20 m^2/g, for example supports on the basis of α-Al_2O_3 and various aluminosilicates (cordierite, mullite, etc.) [1,2], which are normally washcoated by γ-alumina for the catalyst preparation [1,4–6]. In practice, during the dry-curing and temperature treatment of the both types of impregnated monoliths in ambient atmosphere, without air circulation through channels, the intensive evaporation of the solvent from the external surface of the monolith takes place. As a result, the solution containing an active component precursor is driven to the external surface of a monolith by capillary forces, which results in a non-uniform distribution of the precursor and subsequently producing non-uniform monolithic catalyst. As one of measures to

* Corresponding author. Tel.: +7 3832 341 219; fax: +7 3832 397352.
E-mail address: ZRI@catalysis.nsk.su (Z.R. Ismagilov).

0920-5861/$ – see front matter © 2005 Published by Elsevier B.V.
doi:10.1016/j.cattod.2005.06.054

prevent this, we normally cover the impregnated monoliths by a polyethylene cloth to exclude concentration of an active component on the external surface. Another possibility is to apply the intensive circulation of air through the channels of a monolith during the dry-curing and thermal treatment.

For the preparation of an optimal catalyst, it is important to have the knowledge on the catalyst precursor solution dynamics during impregnation and drying in different sections of the pore space of a monolithic support, e.g., in the pores of both the bulk monolith substrate and of the washcoated layer.

The ^{1}H-NMR imaging technique allows one to monitor changes in the distribution of proton-containing liquids, including water, in the pore structure of various materials during drying [7,8]. We assume that the dissolved active component precursor does not strongly adsorb to the walls of the monolith channels, and its concentration in diluted aqueous impregnating solutions has negligible effect on the solution viscosity. On this assumption, the water mass transfer visualization by ^{1}H-NMR imaging also makes it possible to visualize the precursor distribution in the pore structure of a monolith. Earlier we have studied drying of a water-saturated alumina honeycomb monolith by purging the dry air through its channels [8]. The registration of one-dimensional projections of water content in axial direction during drying at a low flow rate of dry air has shown the importance of capillary forces, which redistribute the liquid throughout the pore structure of the sample.

In this paper, the ^{1}H-NMR imaging technique was used to study the dependencies of drying dynamics and the active component (Pt, Pd) precursor distribution in the bulk and washcoated honeycomb monoliths on the support pore structure and on the drying conditions. Two-dimensional ^{1}H-NMR images of water content in axial and radial directions of the monolith samples were registered, which makes it possible to visualize transient pictures of the water distribution in the monolith walls and to determine the main parameters affecting the drying dynamics, particularly the effects of the pore structure and drying conditions.

The three parameters were mainly varied: the space velocity of the dry air flow supplied to the lower cross section of a monolith vertically placed in the NMR cavity, uniformity of the air flow regulated by an air flow distributor placed below the lower inlet of a monolith, and accessibility of the external monolith walls to dry air flow.

2. Experimental

2.1. Preparation of honeycomb monoliths

The honeycomb structured monolithic substrates were prepared by the extrusion of molding masses containing γ-Al_2O_3 powder and aluminum hydroxide sol of pseudo-boehmite composition. The extruded monoliths were subjected to the dry-curing at room temperature for several days, drying at 100 °C and calcination at selected temperatures (600, 900, 1200 °C).

The monoliths calcined at 1200 °C and composed of α-Al_2O_3 were used for the preparation of washcoated samples by the deposition of γ-Al_2O_3 suspension, according to an earlier described procedure [9]. The washcoated substrates were calcined at 600 °C. The washcoat content was 20 wt.%, with a thickness of about 60–80 μm.

The alumina monolithic substrates calcined at 600 °C were incipient wetness impregnated by H_2PtCl_6 or H_2PdCl_4 solutions of desired concentrations followed by calcination at 600 °C. The Pt (Pd) loadings measured by IPC-AES were 1 wt.%.

Total pore volume (V_Σ, cm^3/g) was determined by mercury porosimetry in the effective pore radius (r_{ef}) range from 4 to 10^5 nm using a Porosiger-9300 instrument. The volume of pores with radius less than 6000 Å ($V_{<6000A}$, cm^3/g) and specific surface area (S_{BET}) were determined from isotherm of nitrogen adsorption measured at 77 K using ASAP-2400. The main geometrical and physicochemical characteristics of the monoliths and catalysts are presented in Table 1.

2.2. ^{1}H-NMR imaging procedure

For the NMR experiments, the calcined piece of a monolith (diameter 17.5–19.8 mm; length 20 mm) was saturated with water by immersing into it for 8–10 min. Then, the sample was removed from water and blown-through by air to remove excess water droplets present in the monolith channels. The weight of the monolith was registered before and after saturation with water, and in all experiments the weight of adsorbed water corresponded to the pore volume of the monolith determined by mercury porosimetry (Table 1).

The ^{1}H-NMR imaging experiments were performed using a Bruker ''Avance-300'' NMR spectrometer equipped with a microimaging accessory capable of delivering gradient pulses of up to 100 G/cm. More experimental details can be found elsewhere [8,10].

In order to achieve the uniform air flow distribution in the whole cross section of the monolith sample, the sample holding vertical glass tube was modified: the air distributor was placed below the lower front of the monolith in the tube. This distributor was made of a porous reticulated foam material based on mullite-corundum ceramics with 15–20 ppi cell density, 20 mm diameter and 10 mm length.

After saturation with water, a wet sample was placed into the glass tube located in the cell, so that the lower front of the monolith was fixed 2–5 mm higher than the exit edge of the air distributor. Dry air was fed from below, passing through the air distributor and channels of a monolith with volumetric flow rates of 96.7 and 180 cm^3/s, which correspond to the linear velocities of 30.8 and 57.2 cm/s for the monoliths used.

Table 1
Physico-chemical properties of honeycomb monoliths

No.	Designation	Calcination temperature °C	Geometrical adjectives (D; L; wall, mm) (channel density, cpsi)	XRD composition	Mercury porosimetry			Nitrogen adsorption		ρ_{true} (g/cm^3)	ε (%)
					V_Σ (cm^3/g)	R_{ef} (nm)	Fraction of pores with predominant radii (V_R/V_Σ, %)	$V_{<6000A}$ (cm^3/g)	S_{BET} (m^2/g)		
1	Al_2O_3 (600)	600	(19.8; 20.0; 0.5) 100	90% γ-Al_2O_3, 10% α-Al_2O_3	0.44	76	56% (20–100 A)	0.34	145	3.479	0.59
2	Al_2O_3 (900)	900	(19.3; 20.0; 0.5) 100	θ-Al_2O_3, α-Al_2O_3	0.46	110	49% (40–100 A)	0.31	85	3.581	0.59
3	Al_2O_3 (1200)	1200	(17.5; 20.0; 0.4) 156	α-Al_2O_3	0.34	380	58% (220–1230 A)	0.03	10	4.050	0.55
4	γ-Al_2O_3/Al_2O_3 (1200)	600	(19.8; 20.0; 0.5) 100	γ-Al_2O_3, α-Al_2O_3	0.33	235	13% (<83 A) 21% (83–590 A) 40% (590–1230 A)	0.1	41	3.936[a]	0.57
5	1 wt.% Pt/Al_2O_3 (600)	600	(19.8; 20.0; 0.5) 100	90% γ-Al_2O_3, 10% α-Al_2O_3	0.44	76	60% (20–100 A)	0.34	143	–	–
6	1 wt.% Pd/Al_2O_3 (600)	600	(19.8; 20.0; 0.5) 100	90% γ-Al_2O_3, 10% α-Al_2O_3	0.43	76	58% (20–100 A)	0.34	144	–	–

Geometrical adjectives: D and L: diameter and length of monolith, respectively; cpsi: cell per square inch. Mercury porosimetry data: V_Σ: total pore volume, R_{ef}: effective pore radius. Nitrogen adsorption data: $V_{<6000A}$: pore volume with radii smaller 6000 A, S_{BET}: surface area measured by BET. ρ_{true}: true density, ε: porosity.
[a] Calculated value.

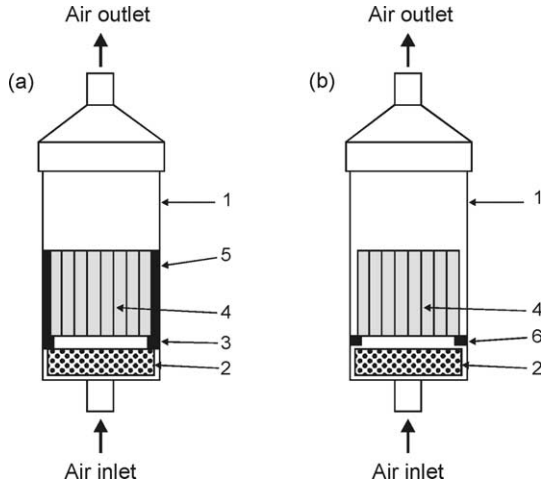

Fig. 1. Sample holder for ^{1}H-NMR imaging experiments. 1-teflon tubing, 2-ceramic air distributor, 3-teflon ring for sample holding, 4-monolith, 5-teflon film coating, 6-teflon shoulders for sample holding.

The drying dynamics was studied for two cases: first when the external walls of a monolith were open and accessible for the air flow, and second with the monoliths external walls covered by teflon film (Fig. 1). In the experiments for imaging the water content in the radial direction of the monolith, the thickness of the analyzed segment at the half of axial direction of the sample was 2 mm. The registration of a full image took 1.97 min. Forty two-dimensional water content maps in axial or radial direction were recorded during each experiment.

3. Results and discussion

3.1. Drying of bulk substrate monoliths.

In the case of incipient wetness impregnation, the active component precursors normally have a macroscopically uniform distribution in the bulk of a support, having the similar distribution map as the solvent–water. However, the distribution of dissolved precursor compounds in the pore structure is significantly changed during the drying, due to the characteristics of capillary transport of the solution. As a first approximation, which neglects the specific adsorption of a precursor compounds on the substrate material one can follow the processes of distribution and redistribution of precursors by registering the dynamics of water content distribution map.

The series of two-dimensional water content distribution maps along the radial and axial directions in the process of drying the alumina monolith preliminarily calcined at 600 °C and saturated by water are presented in Fig. 2. In these series of experiments, the external walls of monoliths were covered by teflon film and were not accessible to the air flow. The water content distribution maps along the sample radial and axial directions, registered upon the same drying duration in different experiments, are in good agreement

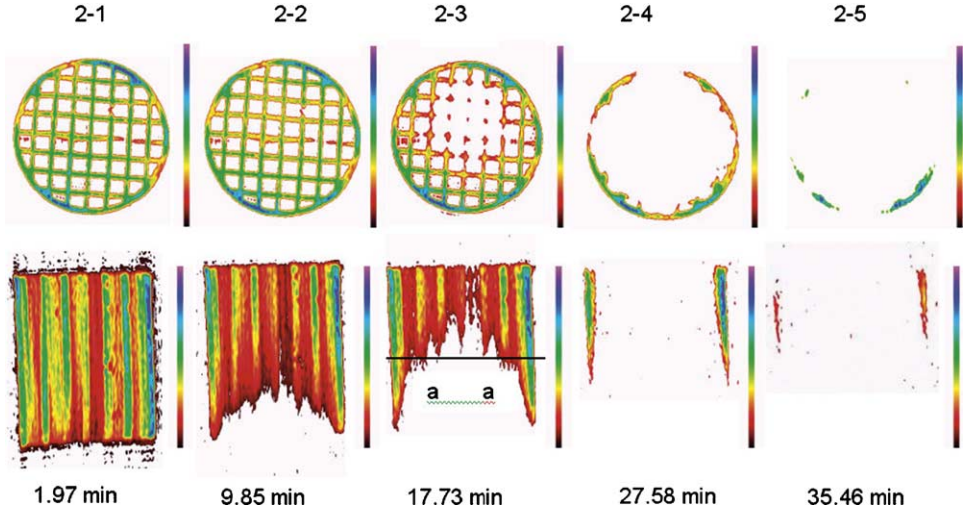

Fig. 2. Two-dimensional water content distribution maps recorded during drying of the alumina monolith calcined at 600 °C. The image registration time is 1.97 min. The air flow rate is 57.2 cm/s. The air does not have access to the external surface of the monolith. Values under the images are times when the image registration ended.

with each other. The first image 2.1 shows that the distribution of water in the sample is not uniform: there is more water in the external wall of the monolith (blue color) than in its central part (yellow-green color). The following images 2.2 and 2.3, registered after 9.85 min and 17.73 min of drying show that the water concentration in the central part of the sample decreases, as indicated by an increase of red and yellow colors in the water content distribution maps in both radial and axial directions. These parabolic profiles characterize higher water content in the external wall because this wall is isolated from external air flow. The images 2.4 (after 27.58 min) and 2.5 (after 35.46 min) characterize practically full drying of the monolith, with the external wall being the last one to dry.

Similar features, in particular fast drying of the central part of the monolith, and slow drying of the external wall were also observed at a lower drying air flow rate (30.8 cm/s). In these experiments, upon decreasing of the drying air flow rate from 57.2 to 30.8 cm/s the drying time was longer: for the samples calcined at 600 °C, the time required for the arch of the water content parabolic curve to reach the half of axial direction of the monolith (a-a section, Fig. 2, image 2.3) increased from 18 to 27.5 min.

In the experiments with the open external wall of monoliths, the two-dimensional water content distribution maps along the radial and axial directions had demonstrated that in this case the drying profile was more uniform (Fig. 3). The drying of the monolith external wall proceeds with almost the same rate as that of the channel walls in the central part of the monolith. Note that for all the samples drying uniformity is improved when a higher dry air flow rate is used. Upon the air flow rate of 57.2 cm/s, the uniform

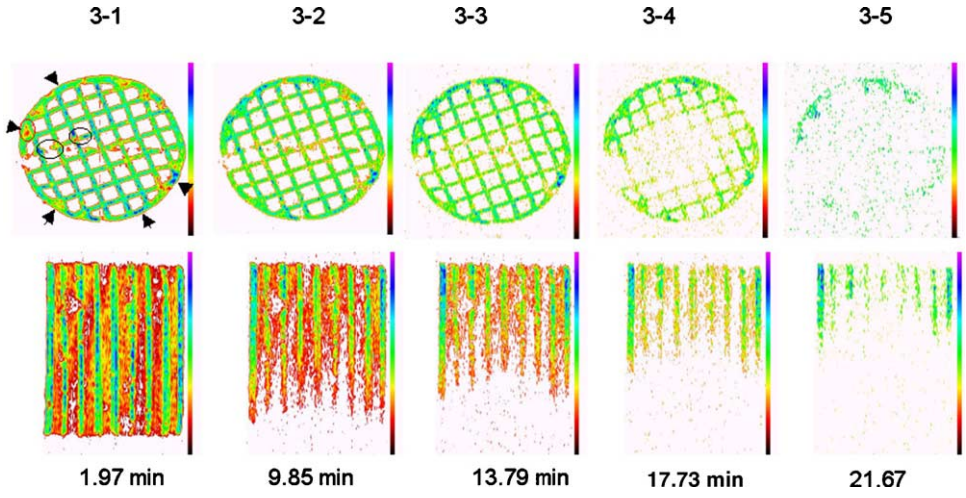

Fig. 3. Two-dimensional water content maps recorded during drying of the sample calcined at 600 °C. The image registration time is 1.97 min. The air flow rate is 57.2 cm/s. The air freely accesses to the external surface of the monolith. Values under the images are times when the image registration ended.

decrease of signal intensity along the sample radial direction is observed, and the parabolic profile along the sample axial direction is expressed weakly. However, despite the drying uniformity in general, the high concentration spots can be found in this case as well, mostly located in thicker segments of the external monolith wall.

Drying of the sample calcined at 1200 °C (Fig. 4B) is faster and more uniform than that of the samples calcined at 600 °C (Fig. 4A). The differences in the drying dynamics of samples upon the increasing of calcination temperature from 600 to 1200 °C are, most likely, due to the sintering of small pores, resulting in the decrease of the total pore volume from 0.44 to 0.29 cm^3/g and growth of the predominating and effective pore radii from 45–50 to 380 Å and from 82 to 960 Å, respectively.

3.2. Drying of washcoated monolith

Several characteristic features observed during the study of the drying dynamics of α-Al_2O_3 monoliths washcoated by γ-Al_2O_3 can be distinguished during analysis of the two-dimensional water content distribution maps along radial and axial directions (Fig. 4C). The images 4C.1 and 4C.2 recorded at the beginning of drying process are characterized by the high intensity of ^{1}H-NMR signal in the center of the monolith walls in comparison with their surface. However, these data do not allow us to unambiguously affirm that there is more water in the wide pores of α-Al_2O_3 monolith than in the narrow pores of γ-Al_2O_3 washcoat, because the ^{1}H-NMR signal intensity in a liquid depends on a spin-lattice relaxation time, T_1. The spin-lattice relaxation

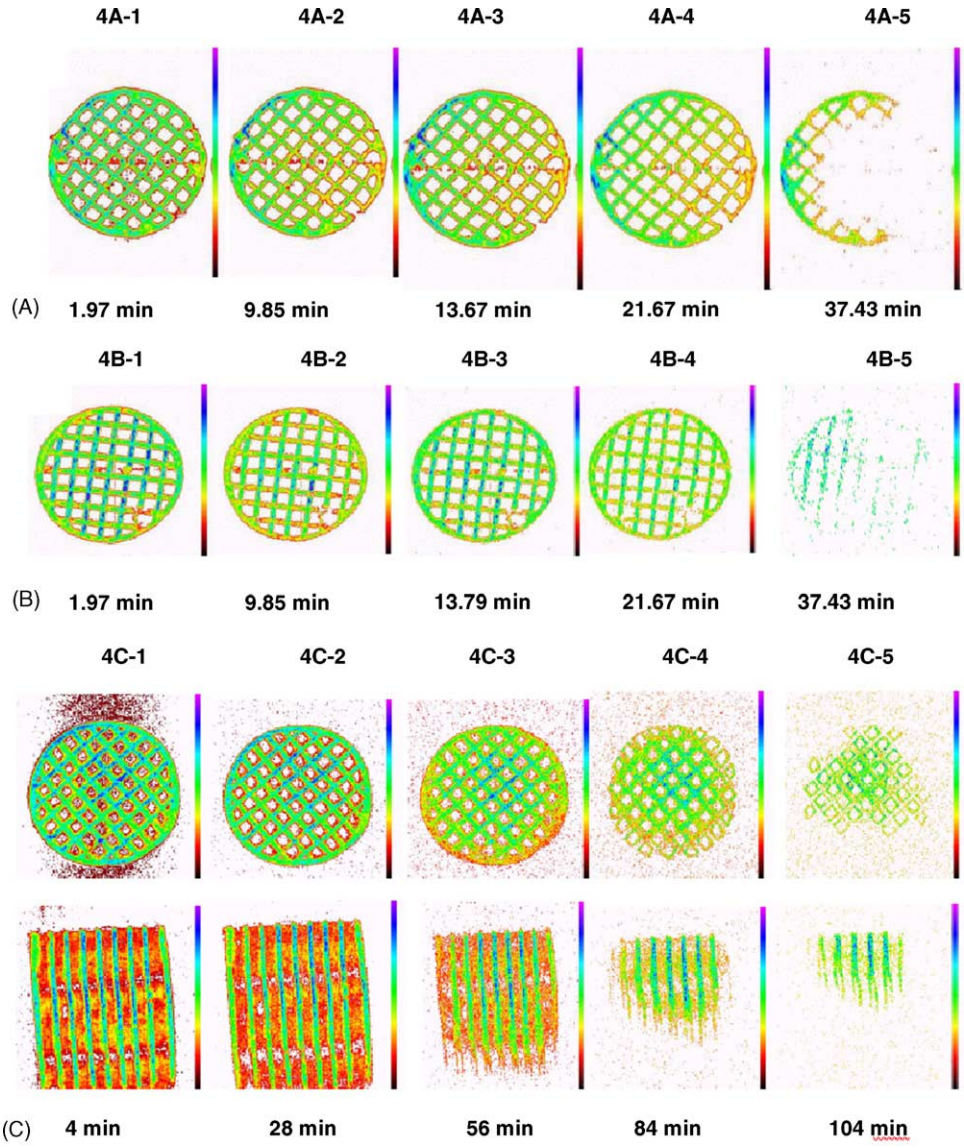

Fig. 4. Two-dimensional water content maps recorded during drying of the parent alumina monoliths calcined at 600 °C (A) and 1200 °C (B) and α-Al_2O_3 monolith washcoated by γ-Al_2O_3 (C). The image registration times are 1.97 min (A, B) and 4 min (C). The dry air flow rate is 30.8 cm/s. The drying air freely accesses the external surface of the monolith. Values under the images are times when the image registration ended.

time of a liquid in the large pores is longer than in the narrow pores. The drying process starts from the external surface of the monolith (maps 4C1–4C3). Then, the signal of the external monolith wall disappears (map 4C4), and the drying process moves to the central part of the monolith (map 4C5). Meanwhile, some water remains in the thin layer of washcoat (maps 4C4, 4C5). In addition, in all the maps one can easily see a ''cellular'' structure of the ^{1}H-NMR image of the washcoat, which is the last one to dry. The observed effect is due to the difference in pore size of the high-temperature α-Al_2O_3 substrate monolith wall and the washcoat, 380 and 45–50 Å, which results in the redistribution of water by capillary forces from the bulk of monolith walls to the washcoat, which dries by water evaporation from the surface of narrow pores.

The observed characteristics of the drying dynamics suggest that during the drying of impregnated washcoated monolith a certain part of the introduced active component precursor is transported from the substrate macropores to the mesoporous washcoating layer. In general, the precursor redistribution and, consequently the size of crystallites formed after drying significantly depend on the support pore structure, especially on the predominating pore radius and drying conditions.

It is important to note that the transfer of the impregnating solution from one end of the monolith to the other, together with the flow of drying air, may lead to the enrichment of the monolith edge face by the precursor. Therefore, to reach a uniform active component distribution along the monolith axial direction, it is necessary to provide the alternating air blow-through direction.

3.3. Spatial distribution of the active component in monoliths

The most interesting subject of the study by the ^{1}H-NMR imaging method is the spatial distribution of an active component precursor in the monolith pore space before and after the heat treatment. The technique used for the determination of active component spatial distribution in the sample is based on the difference of proton nuclear spin relaxation time T_1 in a liquid contained in the sections of sample with the active component and without it. The ^{1}H-NMR signal intensity depends on the spin-lattice relaxation time T_1. Various dissolved compounds may either increase the T_1 of liquids present in the pore volume of substrate (diamagnetic additives, e.g., $PdCl_4^{2-}$, $PtCl_6^{2-}$ [8,11,12]), or, on the contrary, decrease it (paramagnetic additives, e.g., Fe^{3+}, Cu^{2+} [10]).

In the preliminary experiments aimed on the visualization of differences in the detection of water and impregnating solution in the pore space, the two-dimensional T_1-weighed images were simultaneously registered for the two alumina half-monoliths impregnated with pure water and with the solution of active component precursor. The distribution of the impregnating solution in the pore space of a monolith substrate was studied using the aqueous solutions of H_2PtCl_6 (25 mg Pt/ml) and $Pt(NH_3)_4Cl_2$ (5 mg Pt/ml), which correspond to 1 wt.% Pt and 0.25 wt.% Pt content in the dry catalysts. The signal intensity in the regions of substrate impregnated with Pt was found to be higher than in the case of the sample impregnated with water, due to difference in their spin-lattice relaxation time (Fig. 5). Registration of the active component spatial distribution maps shows that in the freshly impregnated substrate before drying, the active component is uniformly distributed. Note that the active component precursor concentration is slightly higher inside the channel walls than on the surface of the walls. One can also see that the intensity of ^{1}H-NMR signal from the half of the sample containing the active component grows with an increase of platinum precursor concentration in the solution (Fig. 5a and b) and is apparently independent on the type of a platinum precursor.

The distribution of active components, namely platinum and palladium oxides, in the honeycomb monolithic catalyst and their influence on the ^{1}H-NMR imaging were studied

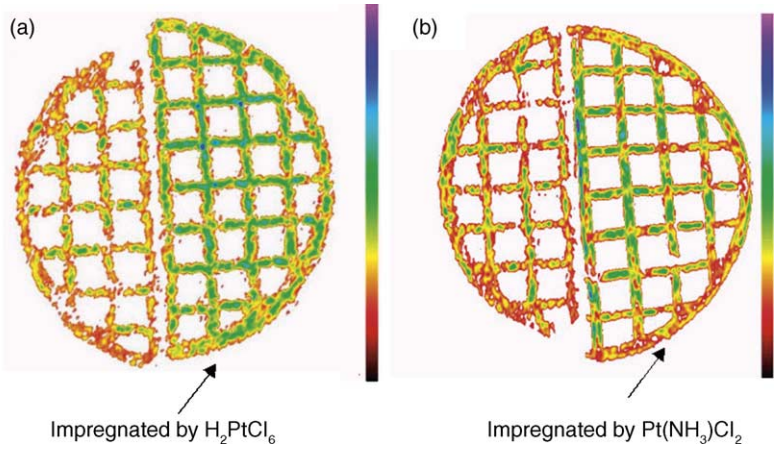

Fig. 5. Comparison of water content distribution maps of two halves of alumina monolith (T_c = 600 °C) impregnated with water and with the active component precursor H_2PtCl_6 (25 mg Pt/ml) or $Pt(NH_3)_4Cl_2$ (5 mg Pt/ml). The Pt loading calculated for dry catalyst was 1% Pt (a) and 0.25% Pt (b). Repetition time is 200 ms.

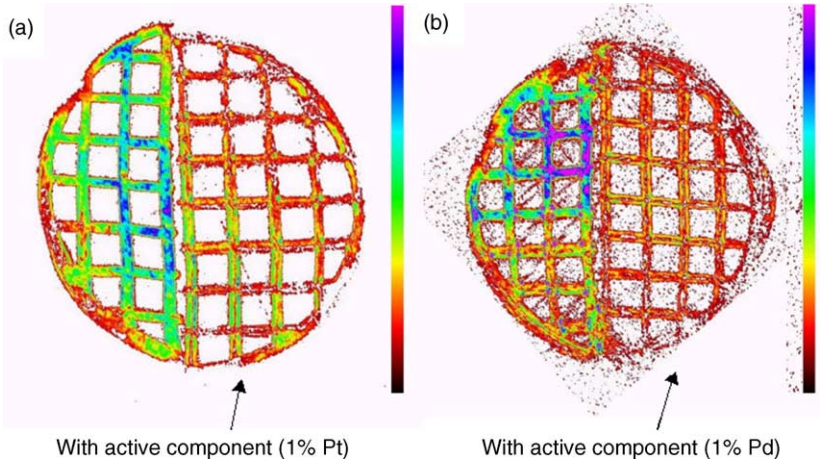

Fig. 6. Comparison of water content distribution maps of two halves of parent monolith (T_c = 600 °C) impregnated by water and calcined (T_c = 600 °C) catalyst containing 1% Pt (a) and 1% Pd (b) active component. Repetition time is 50 ms.

after the calcination of impregnated samples in air at 600 °C. In one experiment, the two halves of the monoliths: a half of the parent alumina substrate and a half of the monolith catalyst containing Pt or Pd active component (∼1 wt.%), both saturated with water, were simultaneously placed in the tubular cell and the T_1-weighted images were recorded (Fig. 6). The ^{1}H-NMR signal intensity was lower in the sample with the active component than in the sample without it, indicating that Pt and Pd oxides decrease the spin-lattice relaxation time. Note that both the parent alumina substrate and the monolith catalysts with active component, having the similar pore volumes and pore size distributions, were treated in water for the same time. This fact excludes the attribution of the observed effect to the smaller amount of liquid in the sample with the active component, and the effects of capillary liquid transfer from one half of the substrate to the other.

There is a sort of a sliced structure of the NMR signal intensity in the intersections of the internal walls of monolith channels and also in between the central and external part of the walls. Currently, available data is not sufficient for the assignment of these images to the egg-shell distribution of an active component in the walls of a monolith substrate. Although the obtained spatial T_1 maps are in good agreement with the Pt (Pd) distribution curves obtained by the X-ray microprobe method, we have to collect more experimental data and the work is in progress.

4. Conclusions

The drying dynamics of the γ-Al_2O_3 and α-Al_2O_3 monolithic substrate and the washcoated γ-Al_2O_3/α-Al_2O_3 monolith were visualized by ^{1}H-NMR imaging.

Distribution of water in the impregnated substrate is not uniform, there is more water in the external wall of the monolith than in its central part. During drying of the substrate with covered external walls by blow-through air, the water content in the central part of sample decreases faster both along the sample's radial and axial directions. The two-dimensional water content distribution maps have a parabolic profile.

Drying of the monoliths with open external walls proceeds more uniformly both in radial and axial directions.

The drying of the sample calcined at 1200 °C (α-Al_2O_3) is faster and more uniform than that of the samples calcined at 600 °C (γ-Al_2O_3) due to a difference in the pore structure and pore distribution.

During drying of impregnated washcoated monoliths, a certain part of the introduced precursor is transported from the substrate macropores to the mesoporous washcoating layer and leads to enrichment of the washcoat of the final catalyst by an active component.

The non-destructive character of ^{1}H-NMR microimaging demonstrated its capability to visualize the water content maps in monoliths in the presence of Pt and Pd.

Acknowledgement

This work was supported by the Grants INCO–COPERNICUS contract no. ICA2-CT-1999-10028, INTAS-00413, NWO-RFBR 047.015.012.

References

[1] A. Cybulski, J.A. Moulijn, Catal. Rev. Sci. Eng. 36 (2) (1994) 179.
[2] J.L. Williams, Catal. Today 69 (2001) 3.
[3] Z.R. Ismagilov, S.A. Yashnik, N.V. Shikina, I.P. Andrievskaya, S.R. Khairulin, V.A. Ushakov, I.A. Ovsyannikova, J.A. Moulijn, I.V. Babich, Chem. Sustainable Dev. 11 (2003) 75.
[4] R.M. Heck, S. Gulati, R.J. Farrauto, Chem. Eng. J. 82 (2001) 149.
[5] T.A. Nijhuis, M.T. Kreutzer, A.C.J. Romijn, F. Kapteijn, J.A. Moulijn, Chem. Eng. Sci. 56 (2001) 823.
[6] S.A. Yashnik, V.V. Kuznetsov, Z.R. Ismagilov, V.V. Ushakov, N.M. Danchenko, S.P. Denisov, Top. Catal. 30–31 (2004) 293.

[7] I.V. Koptyug, R.Z. Sagdeev, L.Yu. Khitrina, V.N. Parmon, Appl. Magn. Reson. 18 (2000) 13.
[8] I.V. Koptyug, L.Yu. Ilyina, A.V. Matveev, V.N. Parmon, R.Z. Sagdeev, Khim. Fizika 21 (2002) 68 (in Russian).
[9] Z.R. Ismagilov, R.A. Shkrabina, D.A. Arendarskii, N.V. Shikina, Kinet. Katal. 39 (1998) 600 (in Russian).
[10] I.V. Koptyug, S.I. Kabanikhin, K.T. Iskakov, V.B. Fenelonov, L.Yu. Khitrina, R.Z. Sagdeev, V.N. Parmon, Chem. Eng. Sci. 55 (2000) 1559.
[11] L.Yu. Khitrina, I.V. Koptyug, N.A. Pakhomov, R.Z. Sagdeev, V.N. Parmon, J. Phys. Chem. B 104 (2000) 1966.
[12] B. Boddenberg, B. Beerwerth, J. Phys. Chem. 93 (1989) 1440.